Acta Oncologica Vol. 31, No. 8, pp. 833–842, 1992

CONTRAST-ENHANCED MAGNETIC RESONANCE IMAGING OF THE BREAST

INGRID S. GRIBBESTAD, GUNNAR NILSEN, HANS FJØSNE, REIDUN FOUGNER, OLAV A. HAUGEN, STEFFEN B. PETERSEN, PETER A. RINCK and STENER KVINNSLAND

Contrast-enhanced magnetic resonace imaging (MRI) of 28 patients with known breast tumors was compared with clinical findings and histopathology, and for 12 of the patients also with mammography. The dynamic measurements performed in 18 patients showed that signal intensity in gradient echo (FFE) images increased rapidly in malignant tumors after contrast injection and reached a plateau level at 1–3 min postcontrast. Fibroadenomas showed slower contrast enhancement continuing throughout the whole examination period of 10 min. The most enhancing parts of the tumors were selected for intensity measurements. The differentiation between malignant and benign tumors in dynamic contrast-enhanced MRI was in accordance with the histopathological findings in all cases. The tumor diameter as measured by MRI showed very good agreement with the size of the tumor specimens. Comparison of tumor size measurements in mammography and MRI showed that MRI had the most accurate correlation to the measured size of the tumor specimens.

Several imaging techniques are available for early detection of breast carcinomas. Mammography remains the most effective modality for diagnosis of breast cancer, while magnetic resonance imaging (MRI) is evaluated in order to provide more information in diagnostically difficult cases. After the first MRI studies of the breast were published (1–6), important progress has been made, using T_1-weighted sequences combined with the use of gadopentetate dimeglumine and similar compounds in order to establish MRI as a diagnostic method for breast pathology (7–14), in particular to increase sensitivity and specificity. Studies using single pre- and postcontrast series have shown that all malignancies enhance significantly after intravenous injection of gadopentetate dimeglumine. Absence of enhancement very reliably excludes malignancy (11, 12). Dynamic examinations using gradient echo sequences following contrast enhancement at short-time intervals after injection were proven to yield the most specific information about breast lesions (9, 13). A recent study has shown high sensitivity and specificity in the detection of breast carcinomas, using dynamic measurements (13). Benign lesions also enhance in signal intensity, but with a slower rate than malignant tumors (9, 13).

The purpose of the present study was to evaluate contrast enhancement in MR images after intravenous injection of gadopentetate dimeglumine according to increase in signal intensity (SI) as well as the pattern and rate of enhancement, and to compare the results to clinical findings, receptor analysis, mammography, and histopathology.

Received 9 March 1992.
Accepted 27 August 1992.
From the MR-Center: Natural Sciences Section, SINTEF UNIMED (I.S. Gribbestad, S.B. Petersen) and Medical Section (G. Nilsen, P.A. Rinck)); and Departments of Surgery (H. Fjosne), Pathology (O. A. Haugen), Radiology (R. Fougner), and Oncology and Radiotherapy (S. Kvinnsland), University Hospital, Trondheim, Norway.
Correspondence to: Dr Ingrid S. Gribbestad, MR-Center, Natural Sciences Section, SINTEF UNIMED, N-7034 Trondheim, Norway.

Material and Methods

Twenty-eight female patients with clinically known breast lesions underwent MRI before surgery. The selection was made among patients with palpable tumor size >1 cm. All of them were referred to breast surgery at our hospital. Only the clinical localization of the tumor was known to the MRI examiners.

The patients were examined using a Philips Gyroscan S15 unit operating at 1.5 T. Single breast receiver coils with a diameter of 16, 12 or 8 cm were used, depending on the size of the breast. The circular coil was chosen in order to surround the breast as closely as possible without compressing it. The patients were placed in prone position. The pulse sequences used were either spin echo (SE) sequences or a gradient echo sequence (FFE) (15). The examination protocol consisted of a SE sequence (TR 235/TE 20, 3 transversal sections) to determine the position of the breast in the coil. Sagittal SE images (TR 450-550/TE 20) of the entire breast were obtained with a slice thickness of 7–8 mm to establish location of pathology. One slice in the pathological area was imagined again using the FFE sequence (TR 100/TE 15/flip angle 80°) before and after intravenous contrast injection. This last sequence was a dynamic study consisting of 25 images with a time interval of 30 s. Patient Nos. 1–9 were examined using the sagittal SE sequence before and after contrast injection.

Before the patient was positioned in the magnet a saline drop infusion was started. Gadopentetate dimeglumine (Magnevist, Schering AG, Berlin, Germany, 0.1 mmol/kg body weight) was injected after the first 5 images in dynamic sequence without moving the patient. The contrast injection time was 15–20 s, and was immediately followed by an injection of 10 ml physiological saline solution. Immediately after injection of gadopentetate dimeglumine, 20 images of the same slice in 30 s intervals were made using exactly the same imaging parameters as before the injection. Change of signal intensity in the region of interest was calculated in each postcontrast image and compared to the precontrast value. The automatic scaling of signal intensity was switched off during the dynamic measurements. The increase in signal intensity after the i.v. administration of gadopentetate dimeglumine was calcualted as the percentage increase compared with the signal intensity before the contrast injection, under similar technical conditions (13):

$$\% \text{ increase in SI} = (\text{SI postcontrast/SI precontrast} \times 100\%) - 100\%$$

The signal intensity of the different tissues was measured as an average value within a user defined region of interest (ROI). The ROI was drawn manually in the processed image, and the value was calculated from the drawn area and the slice thickness. Careful selection of the ROI was necessary, in order to select the pixels with the highest contrast enhancement. The value of SI precontrast was calculated as an average of signal intensity measured in 5 images.

A description of the tumor localization and the tumor outline was done independently by the same two radiologists (G.N. and P.A.R.). The tumor outline and pattern of signal enhancement were correlated to the histopathological findings. The largest diameter of the tumor was measured in the postcontrast sagittal images in two directions. The size in the third direction was estimated from the number of slices where the tumor was seen, the slice thickness and the slice gap. The tumor size was compared to the clinically and mammographically determined tumor size, and to the size measured in the tumor specimens.

The estrogen and progesterone receptor levels of the breast tumors were measured using a monoclonal enzyme immunoassay (ABBOTT ER or PgR-EIA Monoclonal). Specimens with values <10 pmol ER or PgR/g protein were considered as negative.

All mammographic examinations were made with a Mamex DC Mag (Soredex/Orion). Three views (oblique, frontal, lateral) were routinely performed. If necessary, additional or magnification views were obtained. The final reading of the mammograms was done by one radiologist (R.F.), having access only to the clinical history of the patients.

Results

Dynamic measurements by MRI

The patient data are listed in Table 1. Dynamic contrast-enhanced MRI was successfully performed in 18 out of 19 patients. One patient did not manage to complete the examination due to generally deteriorated physical condition, and was therefore excluded from this part of the study.

In the precontrast, T1-weighted SE and FFE images, the tumors had low signal intensity. The tumors could often easily be detected when surrounded by fatty tissue (Fig. 1). In dense breasts, the contrast between the tumor and the parenchyma was poor, and the tumor was best seen after injection of contrast medium (Figs 2 and 3). The contrast enhancement appeared higher in the postcontrast FFE images than in the postcontrast SE images (Fig. 3).

All carcinomas enhanced significantly. A signal increase of more than 83% (average: 120% $\pm$ 22%) as compared to the precontrast value was seen within 60 s after injection of gadopentetate dimeglumine (Table 2). The maximum increase in signal intensity was reached within 1–3 min for 12 of the 15 carcinomas. These 12 tumors showed a slow decrease in signal intensity within 8 min compared to the maximum level (Table 2), in the range of 5–25%. The remaining three carcinomas had a corresponding increase in signal intensity during the same period. Measurements

Table 1

Results of tumor size measurements, receptor analysis and histopathology for 28 patients. The stage grouping is according to pathological classification (pTNM).

Patient		Tumor size (mm)				Receptor analysis		Histopathology			
No.	Age	T	pT	Mammography (T)	MRI (T)	ER	PgR	pN(x/y)	G1–3	Diagnosis	Stage
1	76	20 × 25	30*	—	35 × 20	1231	2188	0/11	—	lobular carcinoma	T2N0
2	74	20 × 32	12	25	20 × 16	—	—	0/2	—	lobular carcinoma	T1N0
3	90	32	30*	diffuse	25 × 15	1	1	6/6	3	ductal carcinoma, mucinous	T2N1
4	65	70 × 110	⩾50*	—	80 × 50	758	1	8/8	3	ductal carcinoma	T3N1
5	73	50	40*	—	30 × 25	10	1	4/8	3	ductal carcinoma	T2N1
6	74	35	19*	—	20 × 20	15	1	0/4	2	ductal carcinoma	T1N0
7	68	40	25	—	20 × 15	1	1	0/10	3	ductal carcinoma	T2N0
8	64	23 × 21	15	—	15 × 15	514	197	0/10	2	ductal carcinoma	T1N0
9	31	55	30	40	30 × 25	—	—	0/14	3	ductal carcinoma	T2N0
10	64	43 × 38	30 × 40*	—	31 × 22	3	<1	0/8	3	ductal carcinoma	T2N0
11	54	55 × 55	35	40	30 × 25	6	<1	2/8	2	ductal carcinoma	T2N1
12	70	25	20	20	22 × 23	417	333	0/9	2	ductal carcinoma, mucinous	T1N0
13	51	50	45*	40	40 × 30	188	172	1/8	3	ductal carcinoma	T2N1
14	46	70 × 90	50*	50 × 30	58 × 22	61	29	11/11	3	ductal carcinoma	T2N1
15	84	50	30 × 15*	—	22 × 25	219	101	—	2	ductal carcinoma, mucinous	T2N0
16	71	40	15	23	15 × 15	565	154	1/11	2	ductal carcinoma	T1N1
17	37	25 × 30	15*	80	19 × 25	134	4	0/10	1	extensive, intraductal carcinoma and ductal carcinoma	T1N0
18	76	25	20*	—	17 × 18	64	16	—		fibroadenoma	
19	76	44 × 40	40*	40	45 × 40	13	<1	0/3	—	extensive, intraductal carcinoma	T_{is}
20	53	40	40 × 20*	—	20 × 17	13	44	0/6	3	ductal carcinoma	T2N0
21	75	40 × 35	30*	35	25 × 21	429	168	—	2	ductal carcinoma	T2N0
22	40	20	21	—	19 × 20	22	146	—	—	fibroadenoma	
23	44	32	25	—	23 × 21	5	5	0/11	—	medullary carcinoma	T2N0
24	45	25	15	—	19 × 14	51	54	0/5	2	ductal carcinoma	T1N0
25	57	24	13	15 × 25	18 × 14	161	83	0/8	2	ductal carcinoma	T1N0
26	59	65 × 70	50	—	53 × 40	62	14	12/12	3	ductal carcinoma	T2N1
27	25	22	22*	—	20 × 19	9	97	—	—	fibroadenoma	—
28	67	30	23*	—	30 × 24	201	1396	0/13	2	ductal carcinoma	T2N0

* Tumor size measured at surgery.

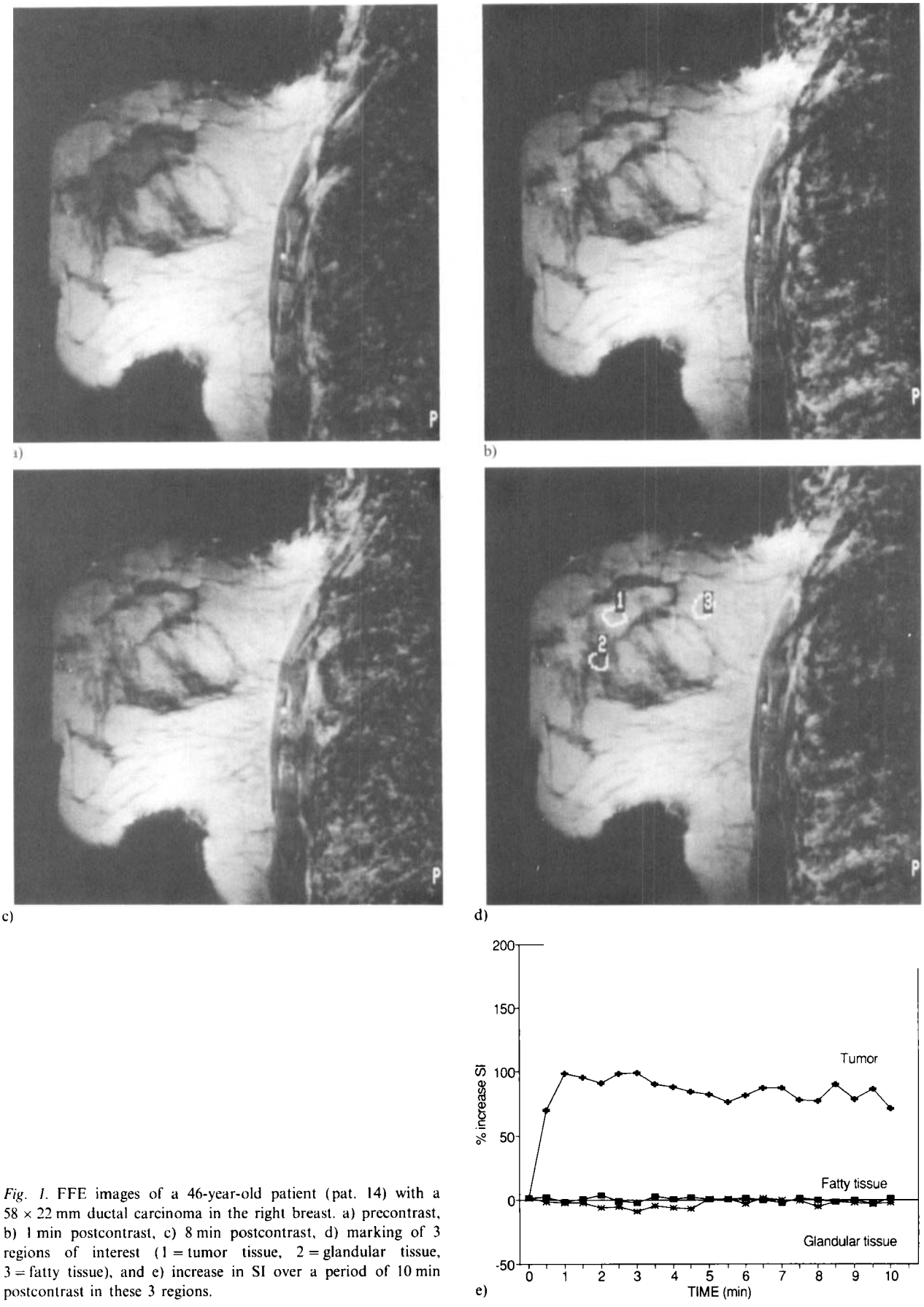

Fig. 1. FFE images of a 46-year-old patient (pat. 14) with a 58 × 22 mm ductal carcinoma in the right breast. a) precontrast, b) 1 min postcontrast, c) 8 min postcontrast, d) marking of 3 regions of interest (1 = tumor tissue, 2 = glandular tissue, 3 = fatty tissue), and e) increase in SI over a period of 10 min postcontrast in these 3 regions.

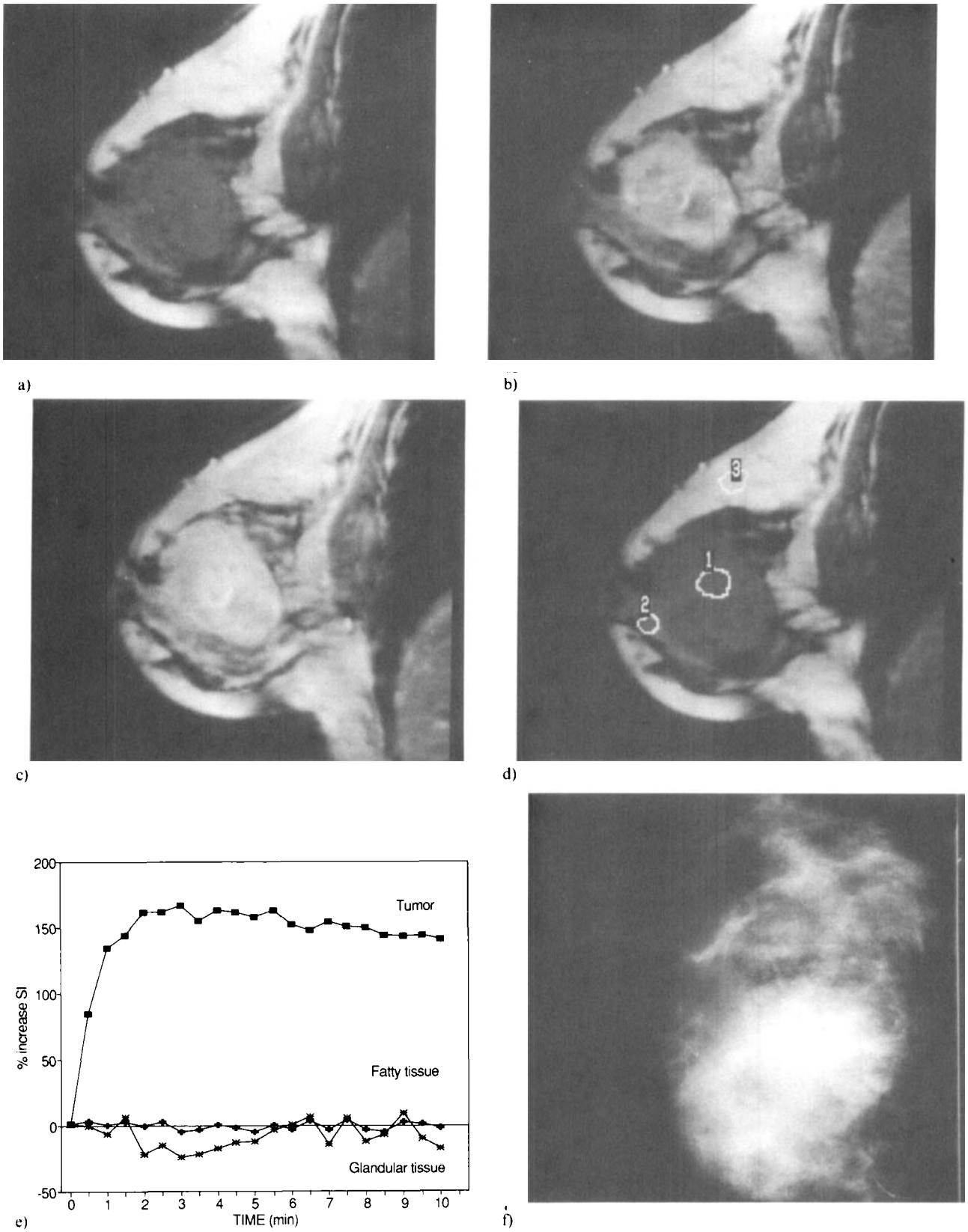

Fig. 2. FFE images of a 51-year-old patient (pat. 13) with a 40 × 30 mm ductal carcinoma in the right breast. Anatomical details are well differentiated, as the chest wall, the pectoralis muscle and different tissues in the breast. The resolution of these images is 0.9 × 0.9 × 7.0 mm. a) precontrast, b) 1 min postcontrast, c) 8 min postcontrast, d) marking of 3 regions of interest (1 = tumor tissue, 2 = glandular tissue, 3 = fatty tissue), e) increase in SI over a period of 10 min postcontrast in these 3 regions, and f) mammogram, lateral view, showing a large lesion without microcalcifications.

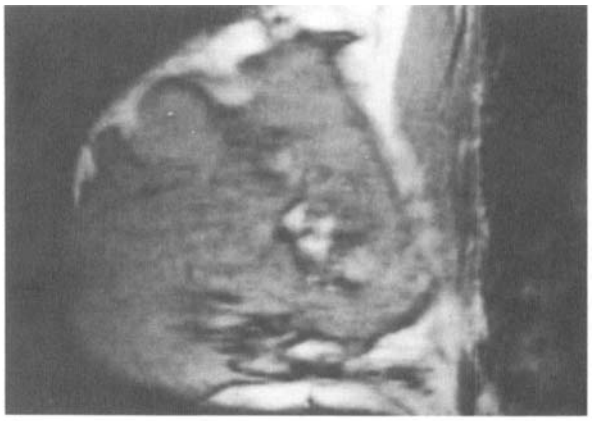

a)

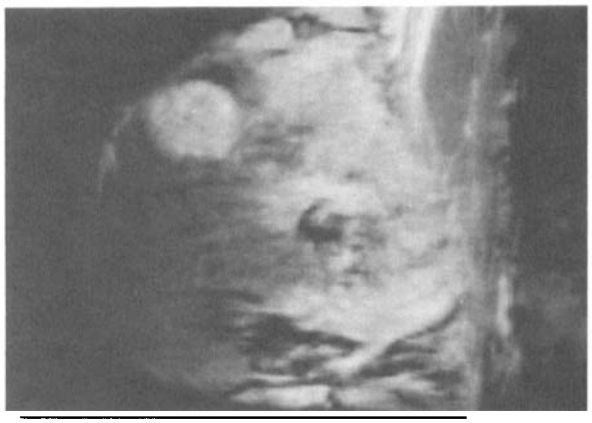

c)

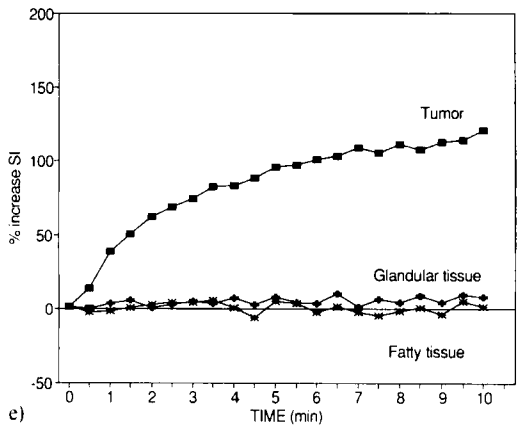

e)

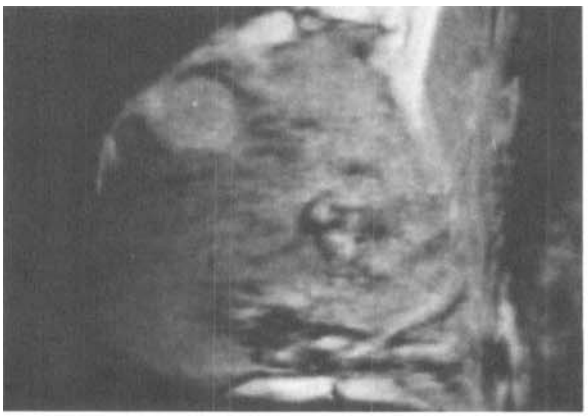

b)

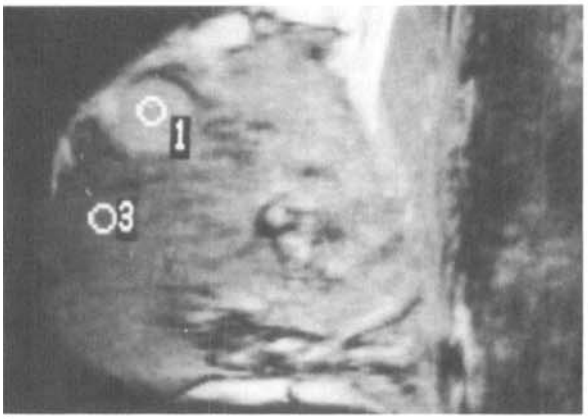

d)

f)

g)

Fig. 3. FFE images of a 25-year-old patient (pat. 27) with a 20 × 19 mm fibroadenoma in the right breast. a) precontrast, b) 1 min postcontrast, c) 8 min postcontrast, d) 3 regions of interest (1 = tumor tissue, 2 = fatty tissue, 3 = glandular tissue), e) increase in SI over a period of 10 min postcontrast in the 3 regions of interest, f) T1-weighted SE image of the same slice, precontrast, and g) postcontrast.

Table 2

Increase of signal intensity 1, 2 and 8 min after injection of gadopentetate dimeglumine in 18 breast tumors, and correlation of MRI diagnosis to histopathological findings

Patient		% increase in SI (SD)			Diagnosis	
No.	Age	1 min	2 min	8 min	MRI	Histopathology
10	64	139 (15)	164 (15)	111 (19)	malignant	ductal carcinoma
11	54	83 (9)	125 (5)	114 (7)	malignant	ductal carcinoma
12	70	105 (8)	186 (15)	191 (6)	malignant	ductal carcinoma, mucinous
13	51	134 (8)	162 (9)	150 (8)	malignant	ductal carcinoma
14	46	99 (8)	91 (7)	77 (7)	malignant	ductal carcinoma
15	84	96 (8)	86 (7)	80 (9)	malignant	ductal carcinoma
16	71	148 (14)	147 (15)	132 (15)	malignant	ductal carcinoma
17	37	111 (18)	132 (17)	113 (17)	malignant	extensive, intraductal carcinoma and ductal carcinoma
18	76	14 (13)	36 (14)	77 (12)	benign	fibroadenoma
19	76	156 (17)	169 (19)	178 (19)	malignant	extensive, intraductal carcinoma
20	53	127 (10)	143 (11)	127 (16)	malignant	ductal carcinoma
22	40	22 (12)	28 (13)	51 (12)	benign	fibroadenoma
23	44	137 (15)	160 (20)	135 (15)	malignant	medullary carcinoma
24	45	137 (10)	145 (10)	123 (8)	malignant	ductal carcinoma
25	57	118 (11)	100 (10)	92 (9)	malignant	ductal carcinoma
26	59	119 (18)	110 (16)	101 (15)	malignant	ductal carcinoma
27	25	38 (5)	62 (6)	111 (6)	benign	fibroadenoma
28	67	86 (10)	100 (9)	106 (10)	malignant	ductal carcinoma

showed little or no increase in signal intensity in surrounding fat or glandular tissue.

In the fibroadenomas, an increase of no more than 40% (average: 25% ± 10%) in signal intensity was seen 60 s postcontrast (Table 2). The increase in signal intensity continued throughout the whole period (Fig. 3). The signal intensity reached the same level as the malignant tumors within the measurement period of 10 min.

The tumor shape was grouped in rounded or irregular shape, and the signal pattern as homogeneous or inhomogeneous. Two of the fibroadenomas appeared as rounded while the fibroadenoma of a 76-year-old woman (pat. 18) had irregular outline. Ductal carcinomas had either rounded or irregular outline. The extensive, intraductal and the mucinous ductal carcinomas had irregular outline.

All ductal carcinomas had inhomogeneous signal pattern 2 min postcontrast. The two patients with extensive, intraductal carcinomas, as well as the medullary one and the two mucinous ductal carcinomas had homogeneous enhancement. Two of the three fibroadenomas showed inhomogeneous enhancement, while the third one was homogeneous. A ductal carcinoma with inhomogeneous signal enhancement (pat. 20) is shown in Fig. 4. The increase in signal intensity 60 s postcontrast varied from 37% to 127% in 10 different regions of the tumor. Out of 10 user-defined ROIs, 5 areas showed enhancement curves with an average increase in signal intensity of 100% ± 14% after 60 s. The other 5 ROIs showed an average increase in signal intensity of 49% ± 11% at the same time postcontrast, and the increase continued throughout the whole examination period. The difference between the highest and the lowest value 8 min after contrast injection was only 34%.

Comparison of diagnostic methods — correlation to tumor characteristics

The diagnosis made from the dynamic contrast-enhanced MRI results was based on an increase in signal intensity 60 s postcontrast using FFE sequences, and development of the contrast enhancement curve throughout the examination period. Increase in signal intensity of more than 70% within this time was interpreted as a suspected malignant tumor. The diagnosis benign tumor was used when the enhancement was less than 70% and the increase in signal intensity continued throughout the whole period. The MRI results based on these criteria correlated to the histopathological findings in all patients.

In patients 1–9 and patient 21, only pre- and postcontrast SE images were made of the tumors. Without any dynamic MRI sequence performed, diagnostic criteria could not be assessed for these tumors. The histopathological findings showed that all of them were malignant tumors.

The results of estrogen and progesterone receptor analysis in 28 patients are listed in Table 1. There were 6

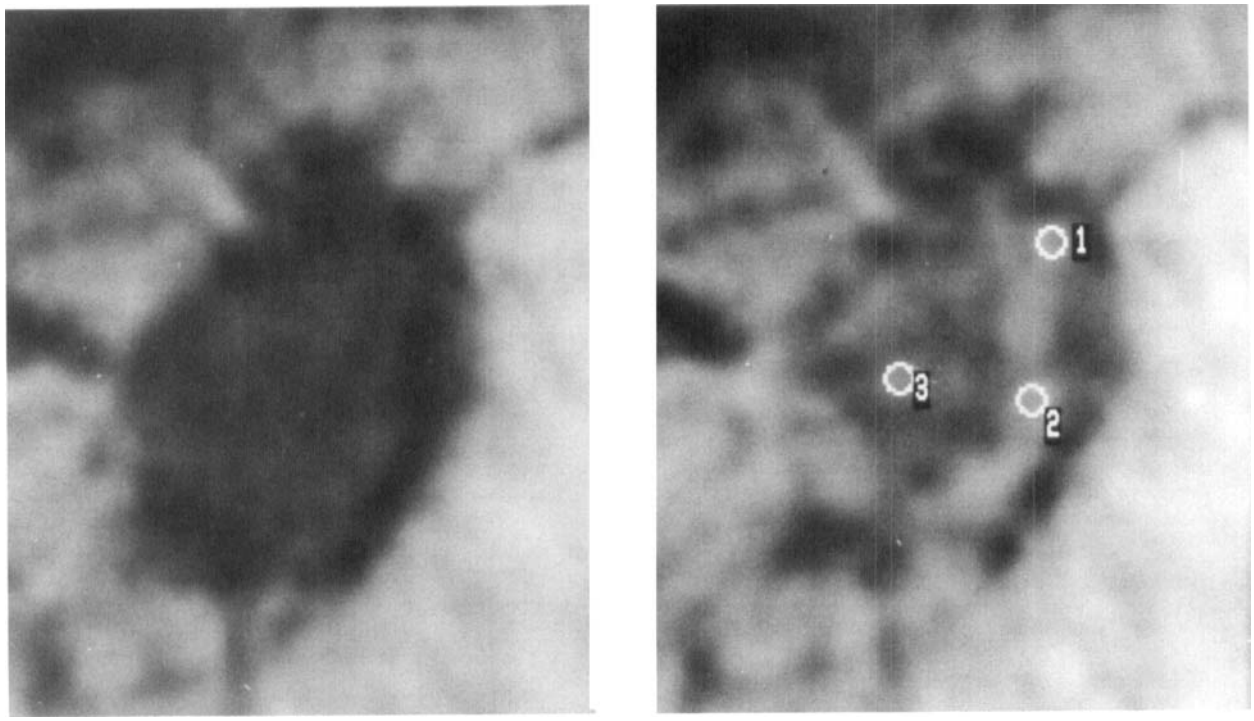

Fig. 4. FFE images of a 53-year-old patient (pat. 20) with a 20 × 17 mm ductal carcinoma in the left breast a) precontrast, b) 2 min postcontrast, with 3 defined ROIs within the tumor, and c) contrast enhancement curves for the 3 ROIs.

patients with ER < 10 pmol/g protein and 10 with PgR < 10 pmol/g protein. No correlation was found when comparing the receptor values and the MRI results.

The histopathological results are listed in Table 1. Even though this study showed no correlation between the increase in signal intensity postcontrast and the histological type of carcinoma, grading of the tumor, or lymph node metastasis, the number of patients is too small for any final conclusion.

Twelve patients underwent mammography at our hospital, and these results were included in the study. Mammography was not performed in 11 patients due to obvious clinical signs of malignancy. Five patients were mammographically evaluated at other institutions and the mammograms therefore not included. Tumor sizes measured in the mammograms are listed in Table 1. All tumors were classified as malignant in the final evaluation of the mammograms, in accordance with the histopathological findings for all the patients. One tumor (pat. 13) was difficult to interpret at the first evaluation. The mammogram from this patient is shown in Fig. 2.

The tumor size was measured in the MR images of 28 patients (Table 1). The accuracy in the two diameters measured in the sagittal image was within ±2 mm. The largest diameter of each tumor found by MRI was compared to the largest diameter found by palpation. In one

case the diameter found by MRI was larger, in 18% of the cases the results matched, and in 79% the measured size in the images was smaller. The maximum deviation was found in a tumor with a palpable size of 40 mm, while the size measured by MRI was 15 mm. The patholgoical size of this tumor was 15 mm. The largest diameter of the tumor measured in the MR images was compared to the pathologically determined tumor diameter in 12 patients (Table 1). The results matched within ± 5 mm, except for patient 2. In this patient, the measured diameter by MRI was 20 mm compared to 12 mm by histopathology. MRI results from the remaining 16 patients were compared to the tumor size determined at surgery (Table 1). In 10 patients the results matched within ± 5 mm, in 3 patients the MRI size was 7–10 mm larger and in 2 patients the MRI size was 9–10 mm smaller. A large deviation was found in one patient (pat. 20), with the measured diameter by MRI being 20 mm compared to 40 mm at surgery. The tumor size measured by mammography and MRI was compared to pathological measurements for 6 patients (Table 1). The MRI results were equal to the pathologically determined tumor size in 5 of the cases, within ± 5 mm. the mammography results were within ± 5 mm in 2 cases, and 8–12 mm larger in 4 cases. Tumor sizes measured at surgery were compared to results obtained by mammography and MRI for 6 patients (Table 1). The MRI results matched within ± 5 mm in 4 cases, and were 8–10 mm larger in another 2 cases. The mammography results matched within ± 5 mm in 4 cases. In one case, the tumor appeared as a diffuse lesion impossible to measure. In the latter case, surgery showed a 15 mm and mammography a 80 mm tumor diameter (MRI 25 mm).

Discussion

All patients were examined in prone position with a circular surface coil surrounding the pending breast, allowing the breast to fall freely into the coil and a good anatomical delineation to be obtained. The examination time was 30–50 min. A few of the patients complained about discomfort or became claustrophobic in the magnet.

Hardware or software restrictions of our MR imager restricted the acquisition of dynamic images to only one slice. The selection of this slice is difficult, since the lesion must be identified in the precontrast images which have poor tissue contrast between tumor and parenchyma. Screening of the whole breast yields a poor time resolution, losing the important information from the first minutes after contrast injection. Technical improvements allowing measurements of more slices with the same time resolution will be of pivotal importance.

The same position of the ROI was kept for all images of a given dynamic sequence. Movement of the breast will yield a different content of tissue in the measured area. In such a case, the ROI should be determined in each image. The variation of the enhancement curve of glandular tissue in Fig. 1 is probably due to such movement of the breast.

Particular care must be taken when drawing the ROI, to ensure that the most enhancing part of the lesion is selected. Half of the results from 10 ROIs measured in the same tumor (Fig. 4) could be interpreted as enhancement curves typical for benign lesions, like the fibroadenomas in our study. A tumor containing areas of necrosis and/or fibrosis will have an inhomogeneous signal intensity with various pattern of signal increase in the different parts of the tumor. A method for selecting the most enhancing part of the tumor using the actual pixel values in the image would improve the diagnostic value of dynamic measurements.

Since the dynamic measurements have a time resolution of 30 s, the contrast agent must be injected quickly. If the speed of the injection varies, the images will be made with different time intervals from the contrast injection, resulting in incorrect comparisons between the patients.

The contrast enhancement appeared higher in postcontrast FFE images compared to postcontrast SE images (Fig. 3). The signal intensity of fatty tissue in SE images was twice the intensity of the contrast-enhanced tumor, while the signal intensity of the enhanced tumor and fatty tissue was similar in the FFE images, making contrast enhancement less conspicuous in SE than in FFE images. Time resolution and conspicuous contrast enhancement are the main advantages of FFE sequences.

Compared to the precontrast value, all the malignant tumors enhanced more than 83% within 60 s after contrast injection. In our study, the increase in signal intensity 2 min postcontrast was $135\% \pm 30\%$ compared to $120\% \pm 22\%$ found by Kaiser (13), and $122\% \pm 31\%$ compared to $110\% \pm 31\%$ after 8 min. The difference in contrast enhancement could depend on a lower number of patients in our study, and slightly different imaging parameters. The maximum increase in signal intensity was reached within 1–3 min for the malignant tumors, with three exceptions. One extensive intraductal carcinoma, one ductal carcinoma grade 2 and one mucinous ductal carcinoma grade 2 showed a plateau level or a slight increase throughout the remaining part of the examination period. A more detailed analysis of the enhancement curves will be the subject of a future project.

The three fibroadenomas included in our study enhanced less than the malignant tumors during the first postcontrast minutes, but reached the same level within an examination period of 10 min. Compared to the results published by Kaiser (13), the increase in signal intensity 60 s postcontrast was less in our study. Two of our fibroadenomas (pat. 18 and pat. 22) contained a large amount of fibrous tissue, while the fibroadenoma with the highest increase in signal intensity 60 s postcontrast was of juvenile type (pat. 27).

The differentiation between malignant and benign lesions based on dynamic MRI measurements was in agreement with the histopathological findings in all cases. Larger studies are needed to evaluate the sensitivy and specificity of this method in characterization of small tumors and mammographically difficult cases. Higher degree of vascularization has been proposed as the explanation of the much faster contrast enhancement in malignant tumors (10, 13). The question of whether malignant tumors have different amount and differentiation of capillary vessels are now evaluated by histopathological studies and correlated to increase in signal intensity. Other physiological parameters, like the osmotic pressure of the tumor and the content of albumin, will probably also influence the contrast enhancement.

All ductal carcinomas had an inhomogeneous signal appearance 2 min postcontrast, while the mucinous and medullary carcinomas had a homogeneous signal appearance. These results on relatively large tumors indicate that the signal pattern might give some information on the histological type of tumor. No clear differentiation between tumor types could be found when comparing tumor outline in the MR images. A larger number of examinations is needed in order to evaluate the significance of these results.

The tumor size and the exact localization of the tumor provide important information in planning for surgery, especially in order to evaluate the possibilities for breast conserving surgery. In many cases estimation of tumor size by palpation is difficult. Comparison of the largest tumor size measured by palpation and MRI, showed larger values for the clinically determined tumor size in most cases. There was a good correlation between the tumor size measured in the MR images and the size determined by pathology, 11 out of 12 results matched within ± 5 mm. In the one case with a larger deviation (8 mm), only SE images were made of the tumor. These results indicate that MRI is a good method for measurement of the tumor size and for describing the delineation of the tumor. A multislice FFE postcontrast sequence should give an even more exact measure of tumor size.

The number of scientific reports on the use of MRI for breast cancer diagnostics are increasing (16-24). However, the clinical significance of MRI for breast tumor characterization and lesion detection remains to be seen.

ACKNOWLEDGEMENT

This work has been supported by the Norwegian Cancer Society.

REFERENCES

1. Mansfield P, Morris PG, Ordidge R, Coupland RE, Bishop HM, Blamey RW. Carcinoma of the breast imaged by nuclear magnetic resonance (NMR). Br J Radiol 1979; 52: 242-3.
2. Ross RJ, Thompson JS, Kim K, Bailey RA. Nuclear magnetic resonance imaging and evaluation of human breast tissue: preliminary clinical trials. Radiology 1982; 143: 195-205.
3. El Yousef SJ, Alfidi RJ, Duchesneau RH, et al. Initial experience with nuclear magnetic resonance (NMR) imaging of the human breast. J Comput Assist Tomogr 1982; 7: 215-8.
4. El Yousef SJ, Duchesneau RH, Alfidi RJ. Magnetic resonance imaging of the breast. Radiology 1984; 150: 761-6.
5. Heywang SH, Frenzl G, Edmaier M, Eiermann W, Bassermann R, Krischke I. Kernspintomographie in der Mammadiagnostik. Fortschr Röntgenstr 1985; 143: 207-12.
6. Kaiser WA, Zeitler E. Kernspintomographie der mammaerste klinische ergebenisse. Röntgenpraxis 1985; 38: 256-62.
7. Heywang SH, Hahn D, Schmidt H, et al. MR imaging of the breast using gadolinium-DTPA. J Comput Assist Tomogr 1986; 10: 199-204.
8. Revel D, Brasch RC, Paajanen H, et al. Gd-DTPA contrast enhancement and tissue differentiation in MR imaging of experimental breast carcinoma. Radiology 1986; 158: 319-23.
9. Kaiser WA, Zeitler E. MR imaging of the breast: fast imaging sequences with and without Gd-DTPA. Radiology 1987; 165: 120.
10. Kaiser WA, Zeitler E. MR imaging of the breast: fast imaging sequences with and without Gd-DTPA. Radiology 1989; 170: 681-6.
11. Heywang SH, Wolf A, Pruss E, Hilbertz T, Eiermann W, Permanetter W. MR imaging of the breast with Gd-DTPA: use and limitations. Radiology 1989; 171: 95-103.
12. Heywang-Koebrunner SH. Contrast-enhanced MRI of the breast. Schering, 1990; 1-244.
13. Kaiser WA. Dynamic magnetic resonance breast imaging using a double breast coil: An important step towards routine examination of the breast. Front Eur Radiol 1990; 7: 39-68.
14. Kaiser WA. MR mammography (MRM). Medica Mundi 1991; 36: 168-82.
15. Rinck PA, editor. An introduction to magnetic resonance in medicine. Stuttgart, New York: Georg Thieme Verlag, 1990, 42-85.
16. Ravid M, Itzchak Y, Degani H. MR imaging of the physiologic changes of the breast. Radiology 1989; 173: 354.
17. Heywang SH, Hilbertz T, Beck R, Bauer WM, Eiermann W, Permanetter W. Gd-DTPA enhanced MR imaging of the breast in patients with postoperative scarring and silicon implants. J Comput Assist Tomogr 1990; 14: 348-56.
18. Heywang-Koebrunner SH, Beck R, Hilbertz T, et al. Needle localization of breast lesions detected by MR imaging. Radiology 1990; 177: 189.
19. Merchant TE, Kievit HCE, Beijerink D, van der Putte SCJ, de Graaf PW. MRI appearance of multiple papilloma of the breast. Breast Cancer Res Treat 1991; 19: 63-7.
20. Schnapf DJ, Dabb R, Wilson D, Schultze-Haakh H, McGlone J. MR imaging of the reconstructed breast. Radiology 1989; 173: 229.
21. Heywang SH, Beck R, Hilbertz T, et al. MR imaging with Gd-DTPA in the breast after limited surgery and radiation therapy. Radiology 1989; 173: 230.
22. Chacko AK, Totterman S, Rubens D, et al. Paramagnetic accentuation by chemical shift imaging in the breast: improvement in lesion visualization. Radiology 1989; 173: 354.
23. Zobel BB, Tella S, Patrizio G, Confalone D, D'Archivio C, Passeriello R. MR STIR imaging versus spin-echo imaging of the breast: lesion characterization. Radiology 1989; 173: 354.
24. Harms SE, Pierce WB, Flaming DP, et al. New method for breast MR imaging: Fat-suppressed steady-state three-dimensional. Radiology 1991; 181: 134.